Hindawi Publishing Corporation
Journal of Nanomaterials
Volume 2016, Article ID 9182024, 9 pages
http://dx.doi.org/10.1155/2016/9182024

Hindawi

Research Article

Mechanosynthesis of MFe_2O_4 (M = Co, Ni, and Zn) Magnetic Nanoparticles for Pb Removal from Aqueous Solution

America R. Vazquez-Olmos,[1] Mohamed Abatal,[2] Roberto Y. Sato-Berru,[1] G. K. Pedraza-Basulto,[2] Valentin Garcia-Vazquez,[3] Arianee Sainz-Vidal,[1] R. Perez-Bañuelos,[4] and A. Quiroz[2]

[1]*Centro de Ciencias Aplicadas y Desarrollo Tecnológico, UNAM, Circuito Exterior, S/N, Ciudad Universitaria, A.P. 70-186, Delegación Coyoacán, CP 04510, Ciudad de México, Mexico*
[2]*Facultad de Ingeniería, UNACAR, CP 24180, Ciudad del Carmen, CAM, Mexico*
[3]*Instituto de Física Luis Rivera Terrazas, BUAP, Apartado Postal J-48, 72570 Puebla, PUE, Mexico*
[4]*Facultad de Ciencias de la Electrónica, BUAP, 18 Sur y Av. San Claudio, Edif. 109, 72570 Puebla, PUE, Mexico*

Correspondence should be addressed to Mohamed Abatal; mabatal@pampano.unacar.mx

Received 30 August 2016; Accepted 12 October 2016

Academic Editor: Kimberly Hamad-Schifferli

Adsorption of Pb(II) from aqueous solution using MFe_2O_4 nanoferrites (M = Co, Ni, and Zn) was studied. Nanoferrite samples were prepared via the mechanochemical method and were characterized by X-ray powder diffraction (XRD), Fourier transform infrared spectroscopy (FTIR), micro-Raman, and vibrating sample magnetometry (VSM). XRD analysis confirms the formation of pure single phases of cubic ferrites with average crystallite sizes of 23.8, 19.4, and 19.2 nm for $CoFe_2O_4$, $NiFe_2O_4$, and $ZnFe_2O_4$, respectively. Only $NiFe_2O_4$ and $ZnFe_2O_4$ samples show superparamagnetic behavior at room temperature, whereas $CoFe_2O_4$ is ferromagnetic. Kinetics and isotherm adsorption studies for adsorption of Pb(II) were carried out. A pseudo-second-order kinetic describes the sorption behavior. The experimental data of the isotherms were well fitted to the Langmuir isotherm model. The maximum adsorption capacity of Pb(II) on the nanoferrites was found to be 20.58, 17.76, and 9.34 $mg \cdot g^{-1}$ for M = Co, Ni, and Zn, respectively.

1. Introduction

Spinel ferrites play an important role in technological applications. Their interesting electrical, magnetic, and dielectric properties make them useful in many applications, such as electronic devices, sensors, memory devices, data storage, and telecommunications [1–9]. Recently, the possibility of preparing ferrites in the form of nanoparticles (NPs) has opened a new and exciting research field with revolutionary applications, not only in electronic technology but also in the fields of biotechnology [10] and water treatment [11], due to their nanometer size, superparamagnetic properties, and a high surface-to-volume ratio [12, 13]. In recent years, NPs have been applied for removing heavy metals and organic pollutants from aqueous solutions [14–18].

Particularly, the environmental release of lead (Pb) can be mainly attributed to industrial wastewater containing lead-acid battery residues. It is known to cause problems like nausea, convulsions, cancer, and coma, among others, upon long-term drinking [19]. The World Health Organization has set an upper limit of 0.05 mg/L for lead in drinking water. Fortunately, lead can be directly recovered from waste and therefore there is a demand of innovative and economical methods that can reduce contamination and regenerate Pb [20].

It is well known that the properties of ferrite materials strongly depend on the synthesis method. Different procedures for ferrite synthesis are described in the literature, including coprecipitation, low-temperature combustion synthesis, sol-gel, mechanical alloying, mechanical activation, and solid-state synthesis [1, 21–28]. The mechanochemical

synthesis can deliver the desired phases and structures in a single step, with high-energy milling conducted in an enclosed activation chamber at room temperature [29, 30]. Usually, the complete formation of spinel ferrites was obtained only after milling followed by sintering, that is, by employing two processing steps. It has been shown that the combined mechanochemical-thermal treatment yields a well ordered spinel phase in ferrites at lower annealing temperatures and shorter durations than those required in conventional ceramic methods [31–33].

The soft mechanochemical method has a great potential for the synthesis of inorganic precursors because of its versatility and simple operational requirements. Soft mechanochemical reactions usually employ surface hydroxyl groups, adsorbed, hydrated, or contained in a hydroxide. Mechanochemical derived precursors exhibit significantly higher reactivity and thus lower the calcination and sintering temperature [34].

In this article, we investigated the effectiveness of $CoFe_2O_4$, $NiFe_2O_4$, and $ZnFe_2O_4$ ferrite nanoparticles, obtained by soft mechanochemical treatment, for removing lead from aqueous solution.

2. Materials and Methods

2.1. Materials. Ferric chloride hexahydrate, $FeCl_3{\cdot}6H_2O$ (98%), nickel chloride hydrate $NiCl_2{\cdot}H_2O$ (99.95%), cobalt(II) chloride hexahydrate, $CoCl_2{\cdot}6H_2O$ (98%), zinc(II) chloride, $ZnCl_2$(99.999%), potassium hydroxide, lead(II) chloride, $PbCl_2$ (99.99%), KOH (99.99%), and acetone $CO(CH_3)_2$ (99.5%) were obtained from Sigma-Aldrich. All chemicals were used without further purification. Ultrapure water (18 MΩ/cm) was obtained from a Barnsted E-Pure deionization system.

2.2. Synthesis of Spinel Ferrite Nanoparticles. 2×10^{-3} moles (0.5406 g) of $FeCl_3{\cdot}6H_2O$ and 1×10^{-3} moles of MCl_2(where M(II) = Co (0.2379 g), Ni (0.1296 g), and Zn (0.1362 g)) were first milled in an agate mortar for ten minutes. Thereafter, 8×10^{-3} moles (0.4489 g) of previously grinded KOH were added. The mixture was milled for approximately thirty minutes until no change was observed. The obtained powders were washed four times with distilled water and two times with acetone. In each case, the product was separated by centrifugation (3000 rpm for 10 min). Finally, the samples were air-dried and then calcined at 800°C for two hours. The chemical reaction carried out is described as

$$2FeCl_3 + MCl_2 + 8KOH \xrightarrow[800^\circ C/2\,hrs]{\text{Milling}} MFe_2O_4 + 8KCl + 4H_2O \quad (1)$$

where M(II) = Co, Ni, and Zn.

2.3. Adsorption Study on $ZnFe_2O_4$, $NiFe_2O_4$ and $CoFe_2O_4$ Ferrite Samples

2.3.1. Kinetics Studies. Batch mode experiments were performed to determine the kinetics removal of Pb(II) by either $ZnFe_2O_4$, $NiFe_2O_4$, or $CoFe_2O_4$. Sorption experiments for the kinetic study were conducted as follows: 0.01 g of each ferrite sample was added to a separate 10 mL of 100 mg/L $PbCl_2$ solution at pH = 2.0. The three mixtures were placed in centrifuge tubes and shaken in a rotary shaker for 5, 15, 30, 60, 120, and 180 min. After each specific contact time, the tubes were centrifuged at 3500 rpm for 5 min to provide the separation between solid and liquid. The concentration of lead metal was determined using a flame atomic absorption spectrometer (AAS, Thermo Scientific iCE 3000 Series). In order to ensure the truthfulness of the results of the products, all experiments were duplicated.

Adsorption efficiency capacity q_t (mg/g) at specified contact time t (min) was calculated using the following expression:

$$q_t(t) = \frac{(C_o - C_t)V}{m}, \quad (2)$$

where C_0 (mg/L) is the initial metal concentration in solution, C_t (mg/L) is the metal concentration in solution at time t, V is the volume of the aqueous phase (L), and m (g) is the mass of the adsorbent.

In this study, the experimental kinetic data were analyzed by applying the pseudo-first-order and pseudo-second-order kinetic models in order to describe the mechanism involved in the sorption process. The pseudo-first-order kinetic model assumes that the controlling step in the adsorption process is mass transfer, which means that the variation of adsorption rate with time is directly proportional to the difference between the equilibrium concentration of the heavy metal in solution and the concentration of the adsorbate on the adsorbent surface. The first-order rate equation is generally expressed as

$$\frac{dq_t}{dt} = k_1(q_e - q_t), \quad (3)$$

where q_t (mg/g) and q_e (mg/g) represent the amount of Pb(II) adsorbed on the adsorbent at time t and at equilibrium time, respectively, and k_1 (min^{-1}) is the rate constant for the pseudo-first-order adsorption. After integrating and applying boundary conditions, the pseudo-first-order equation in linear form is expressed by

$$\ln(q_e - q_t) = \ln(q_e) - k_1 t. \quad (4)$$

Constants k_1 and q_e are calculated from the intercept and slope by plotting $\ln(q_e - q_t)$ versus t. The pseudo-second-order model assumes that the rate limiting step may be the chemical sorption involving valence forces by means of sharing or exchange of electrons between heavy metal ions and adsorbent.

The pseudo-second-order kinetic equation is expressed as

$$\frac{dq_t}{dt} = k_2(q_e - q_t)^2, \quad (5)$$

where q_e (mg/g) and q_t (mg/g) represent again the amount of Pb(II) adsorbed on the adsorbent at equilibrium time and at time t, respectively, and k_2 ($g{\cdot}mg^{-1}{\cdot}min^{-1}$) is the

pseudo-second-order rate constant. By integrating equation (5) and applying boundary conditions, the pseudo-second-order equation in linear form is given by

$$\frac{t}{q_t} = \frac{1}{k_2 {q_e}^2} + \frac{1}{q_e} t, \tag{6}$$

where parameters q_e and k_2 are determined from the slop and intercept of the plotting of t/q_t against t.

2.3.2. Isotherms Studies. For isotherms studies, 0.01 g of either $ZnFe_2O_4$, $NiFe_2O_4$, or $CoFe_2O_4$ ferrite samples was mixed with 10 mL of aqueous solution at pH = 2 for different concentrations of Pb(II) (10, 40, 80, and 100 mg/L). Then, the mixtures were shaken for 180 min in a rotary shaker at room temperature. This pH value was chosen in order to avoid metal precipitation and also because of the high yield shown at this value. The supernatants were centrifuged at 4500 rpm for 5 min and decanted. The concentration of lead metals in the supernatant was analyzed by AAS.

Langmuir and Freundlich isotherm models are commonly used by various researchers to describe the equilibrium of heavy metal ions between solid and solution phases [35]. This allows determining whether the sorption is of a monolayer or multilayer nature, which can be specifically useful to predict the type of adsorption mechanism involved. The Langmuir isotherm model considers that the binding sites are homogeneously distributed on the adsorbent surface and the adsorption takes place at specific homogeneous sites within the adsorbent. The Langmuir equation is expressed as

$$q_e = \frac{q_m K_L C_e}{1 + K_L C_e}, \tag{7}$$

where q_e is the amount adsorbed at equilibrium (mg/g), C_e is the equilibrium concentration (mg/L), K_L is the Langmuir constant related to the affinity of binding site (L/mg), and q_m is the maximum amount of solute adsorbed (mg/g). The constants in the Langmuir isotherm can be obtained from the slope and intercept by plotting $(1/q_e)$ versus $(1/C_e)$ and making use of the above equation rewritten as

$$\frac{1}{q_e} = \frac{1}{q_m} + \frac{1}{q_m K_L} \cdot \frac{1}{C_e}. \tag{8}$$

On the other hand, the Freundlich isotherm is commonly used to describe the adsorption on the heterogeneous surface. The mathematical expression for the Freundlich isotherm is given as

$$q_e = K_F {C_e}^{1/n}, \tag{9}$$

where K_F $(\text{mg/g})(\text{L/g})^{1/n}$ and n are the equilibrium Freundlich constant indicative of the adsorption capacity and the adsorption intensity, respectively [36]. When $n > 1$, the adsorption process is considered favorable. In contrast, for $n < 1$, the bond between the active sites and metal is weaker and, therefore, the sorption nature corresponds to physisorption or ion exchange. The linear form of Freundlich isotherm is given by

$$\ln q_e = \ln q K_F + \frac{1}{n} \ln C_e. \tag{10}$$

Constants K_F and n are obtained from the slope and intercept of the plot of $\ln(q_e)$ versus $\ln(C_e)$.

2.4. Characterization Techniques. The structure and phase identification of $CoFe_2O_4$, $NiFe_2O_4$, and $ZnFe_2O_4$ ferrite samples were done by X-ray diffraction. For this purpose, an APD 2000 PRO X-ray diffractometer was used. XRD patterns of the materials were obtained using CuK_α radiation (λ = 1.5418 Å) at 35 kV and 25 mA and a variation of 2θ = 10° to 70°, with a scanning speed of 0.025 deg/s and a step time of 10 s. The Fourier transformed infrared (FTIR) technique was conducted using a Nicolet Nexus 670 FTIR infrared spectrometer within a range from 4000 to 400 cm^{-1} with a resolution of 4 cm^{-1} in a KBr wafer. Micro-Raman spectra were recorded with an Almega XR dispersive Raman spectrometer. An Olympus microscope, 50 and 0.85 NA (numerical aperture), was used for focusing the laser on solid samples. Raman spectra were accumulated over 25 s with a resolution of 4 cm^{-1}. The excitation source was 532 nm radiation from a Nd:YVO4 laser (frequency-doubled) and the laser power on the sample was 5 mW. Magnetic properties were examined using a Quantum Design PPMS DynaCool-9 System with a vibrating sample magnetometer (VSM) option. Isothermal magnetization (M) versus applied magnetic field (H) measurements, were performed at 300 and 10 K using fields up to ±80 kOe. Saturation magnetization M_s values were calculated through the interception of M versus $1/H$ curve with the vertical axis.

3. Results and Discussion

3.1. Characterization of $ZnFe_2O_4$, $NiFe_2O_4$, and $CoFe_2O_4$ Ferrite Samples. Figure 1 shows the X-ray diffraction spectra of $ZnFe_2O_4$, $NiFe_2O_4$, and $CoFe_2O_4$. Analysis of each XRD pattern using the MATCH program [37] showed the formation of ferrite phases (JCPDS card 89-7412) with the main reflections 2θ at 30.15°, 35.32°, 43.18°, 53.49°, and 57.15°. The corresponding peaks are well indexed to the crystal planes of spinel ferrite (*hkl*) (220), (311), (400), and (511), respectively [38, 39]. A slight shift in the XRD peak position of $ZnFe_2O_4$, $NiFe_2O_4$, and $CoFe_2O_4$ is observed and is attributed to the difference in the ion radius of Zn, Ni, and Co. From Scherrer equation, and taking into account the (311) diffraction peaks, crystallite sizes of 23.8, 19.4, and 19.2 nm were estimated for $CoFe_2O_4$, $NiFe_2O_4$, and $ZnFe_2O_4$, respectively.

The IR spectra of ferrite NPs show two characteristic vibrational modes. The higher wave number υ_1 band is reported to occur between 550 cm^{-1} and 600 cm^{-1} and is caused by the stretching vibrations of the metal-oxygen (M-O) bond in the tetrahedral sites. The lower wave number range is reported to appear between 365 cm^{-1} and 425 cm^{-1} and is attributed to the M-O bond vibrations in the octahedral sites. The different band positions for the tetrahedral and octahedral complexes are due to the different values of the Fe(M)-O bond lengths in their respective sites [22]. In our samples, υ_1 and υ_2 frequencies were observed at 589 cm^{-1} for $CoFe_2O_4$, 596 cm^{-1} and 404 cm^{-1} for $NiFe_2O_4$, and 564 cm^{-1} and 428 cm^{-1} for $ZnFe_2O_4$ (Figure 2). The replacement of

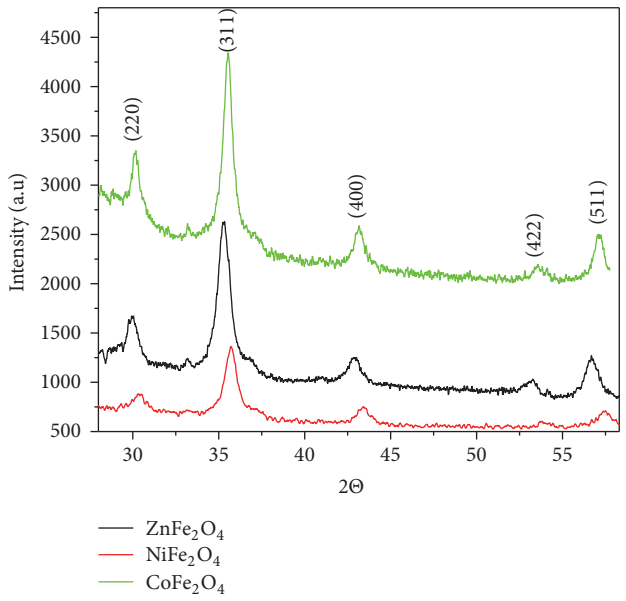

Figure 1: XRD patterns of $ZnFe_2O_4$, $NiFe_2O_4$, and $CoFe_2O_4$.

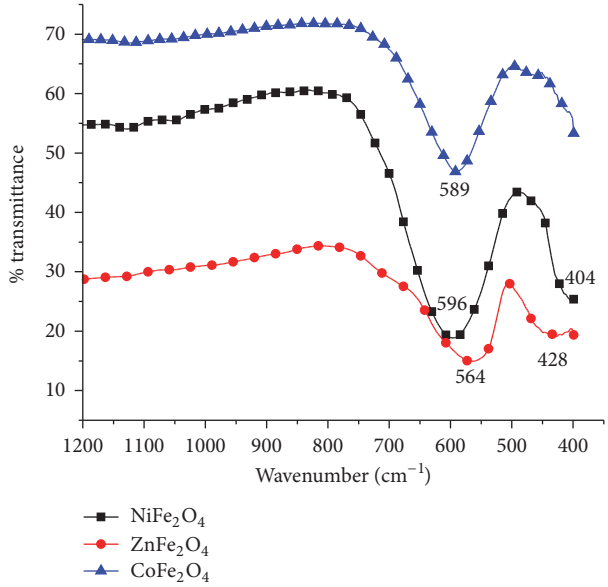

Figure 2: IR spectra of $ZnFe_2O_4$, $NiFe_2O_4$, and $CoFe_2O_4$ nanoparticles.

Co^{2+} by Ni^{2+} or Zn^{2+} has effects on Fe^{3+}-O^{2-} bond. In general, a decrease in wave number and force constant is expected in accordance with the ionic radius increase. $CoFe_2O_4$ and $NiFe_2O_4$ are inverse spinels with tetrahedral sites completely filled with Fe^{3+} and octahedral sites occupied in equal molar amounts by the remaining Fe^{3+} and Ni^{2+} or Co^{2+} cations. This inversion occurs because nickel and cobalt have a higher preference for the octahedral sites than the one iron has. Similarly, $ZnFe_2O_4$ is a normal spinel because Zn^{2+} tends to adopt tetrahedral sites.

Figure 3 shows the room-temperature Raman spectra of $CoFe_2O_4$, $NiFe_2O_4$, and $ZnFe_2O_4$ NPs from 100 cm^{-1} up

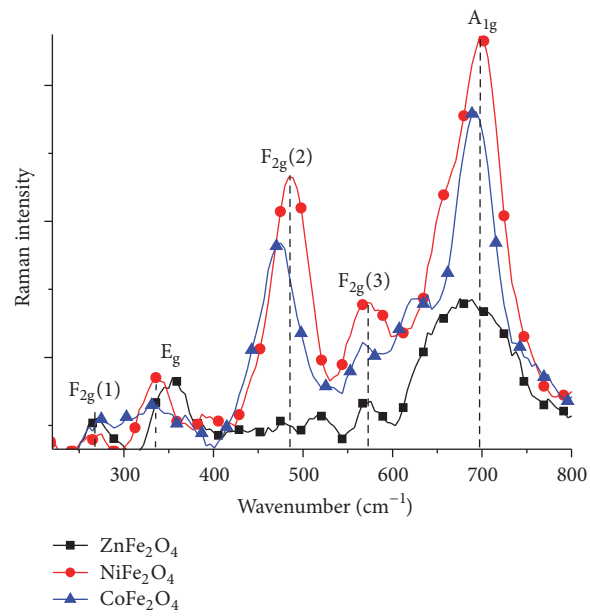

Figure 3: Raman spectra of $ZnFe_2O_4$, $NiFe_2O_4$, and $CoFe_2O_4$ nanoparticles.

to 800 cm^{-1}. Raman spectra of cubic ferrites exhibit five characteristic bands (A_{1g} + E_g + $3F_{2g}$) around 267, 335, 483, 571, and 697 cm^{-1} for $CoFe_2O_4$ and $NiFe_2O_4$ NPs. The A_{1g} mode is due to symmetric stretching of oxygen atoms along Fe-O (or M-O) tetrahedral bonds, E_g and $F_{2g}(3)$ are due to symmetric and asymmetric bending of oxygen with respect to Fe (or M), respectively, and $F_{2g}(2)$ is assigned to asymmetric stretching of Fe(M)-O bond, whereas $F_{2g}(1)$ is attributable to translational movement of the whole tetrahedron [34]. In the Raman spectra of $ZnFe_2O_4$ NPs, however, the bands appear less well defined, and those corresponding to $F_{2g}(2)$ are not observed. In addition, a red shift of the Raman peak is observed because of the optical phonon confinement in these nanoparticles. This behavior has been observed in other metallic oxides when the grain size decreases.

The magnetization (M) versus magnetic field (H) curves are shown in Figures 4 and 5. $NiFe_2O_4$ (Figure 4(a)) and $ZnFe_2O_4$ (Figure 4(b)) NPs do not exhibit hysteresis at 300 K, indicating that both ferrites NPs are superparamagnetic at room temperature. Magnetization levels at 300 K measured at the highest magnetic field, 80 kOe (not shown), are 33.31 and 25.87 emu/g for $NiFe_2O_4$ and $ZnFe_2O_4$, respectively, whereas the saturation magnetization M_s values, calculated by the interception of M versus $1/H$ curve, are 42 ± 0.02 and 39 ± 0.01 emu/g for $NiFe_2O_4$ and $ZnFe_2O_4$, respectively. These values are smaller than the corresponding bulk counterparts [40, 41]. At 10 K, the two samples show a ferromagnetic behavior with coercivity of 713 ± 38 and 913 ± 39 Oe for $NiFe_2O_4$ and $ZnFe_2O_4$, respectively. At 10 K, M_s values for Ni-ferrite and Zn-ferrite samples are 49.16 ± 0.02 and 79.1 ± 0.1 emu/g, respectively.

On the other hand, $CoFe_2O_4$ NPs show a ferromagnetic behavior, with coercivity enhancement at lower temperatures. At 10 K, Co-ferrite nanoparticles exhibit a coercive field

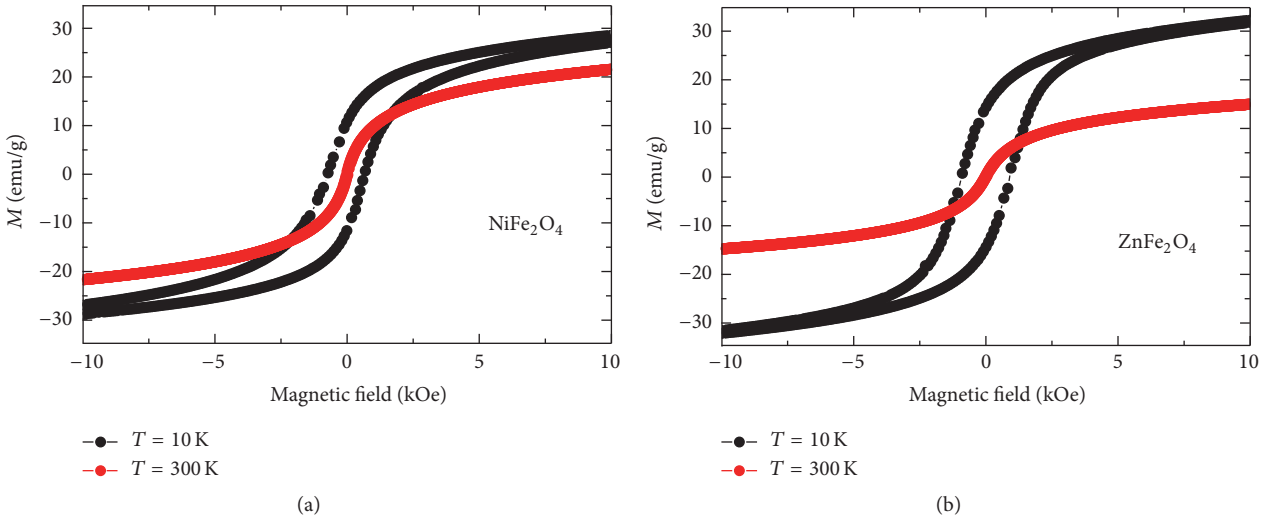

FIGURE 4: Magnetization versus applied magnetic field at 10 and 300 K for (a) $NiFe_2O_4$ and (b) $ZnFe_2O_4$ nanoparticles.

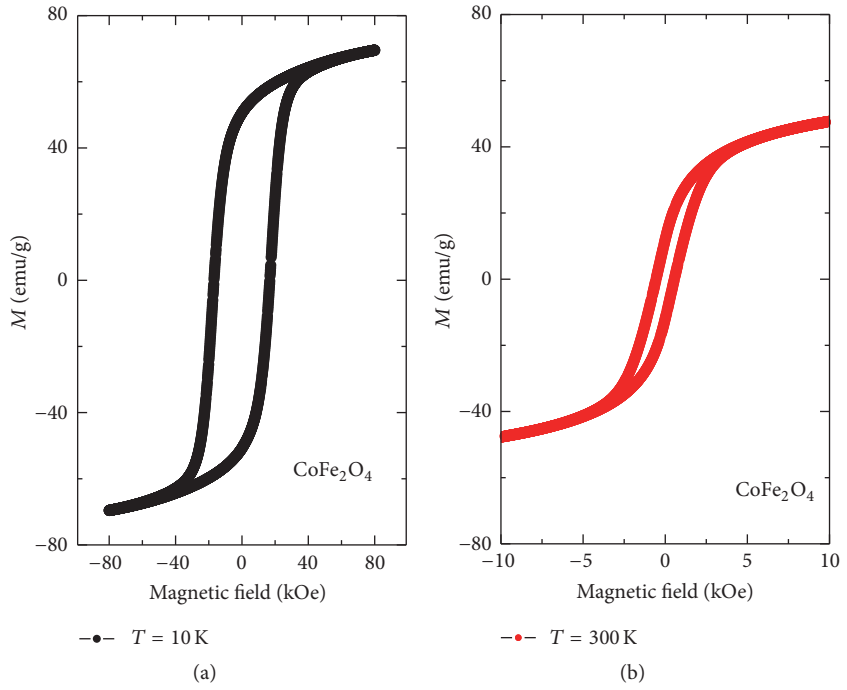

FIGURE 5: Isothermal magnetization curves of $CoFe_2O_4$ nanoparticles measured at (a) 10 K and (b) 300 K.

strength H_c of 16,819 ± 185 Oe (Figure 5(a)), which is much higher than the coercivity found in Ni-ferrite and Zn-ferrite NPs at the same temperature (Figure 4). These results are expected because of the high anisotropy in Co-ferrite. The incorporation of the Co cation in the Fe-O matrix increases the magnetic anisotropy, whereas the incorporation of the Ni or Zn cations reduces it [42]. Saturation magnetization M_s of $CoFe_2O_4$ at 10 K is 80.34 ± 0.02 emu/g, which is very close to that found in $ZnFe_2O_4$ (79.1 ± 0.1 emu/g) at the same temperature. Figure 5(b) shows the magnetization versus field curve of $CoFe_2O_4$ measured at 300 K. The saturation magnetization is 68.3 ± 0.02 emu/g. The magnetization curve of $CoFe_2O_4$ at room temperature exhibits hysteresis, with coercivity of 556 ± 5 Oe. Coercivity enhancement in $CoFe_2O_4$ has been observed by other authors [37, 43, 44]

3.2. Kinetic Study. The removal of Pb(II) for $ZnFe_2O_4$, $NiFe_2O_4$, and $CoFe_2O_4$ nanoparticles was examined at different time intervals and the results are shown in Figure 6(a). As can be seen in this figure, the adsorption capacity of Pb ions with C_i = 100 mgL^{-1} increases rapidly with increasing agitation time up to 30 minutes and then it increases very slowly and becomes nearly constant after 60 minutes. The initial rapid adsorption of Pb(II) can be attributed to the

Table 1: Parameters of the pseudo-second-order kinetic model for $ZnFe_2O_4$, $NiFe_2O_4$, and $CoFe_2O_4$.

Adsorbent type	Pseudo-second-order model			
	k_2 (g.mg^{-1}·min^{-1})	$q_{e,\mathrm{Cal}}$ (mg·g^{-1})	$q_{e,\mathrm{exp}}$ (mg·g^{-1})	R^2
$CoFe_2O_4$	0.095	7.97	7.88	0.999
$NiFe_2O_4$	0.139	11.83	12.02	0.999
$ZnFe_2O_4$	0.389	15.22	15.14	0.999

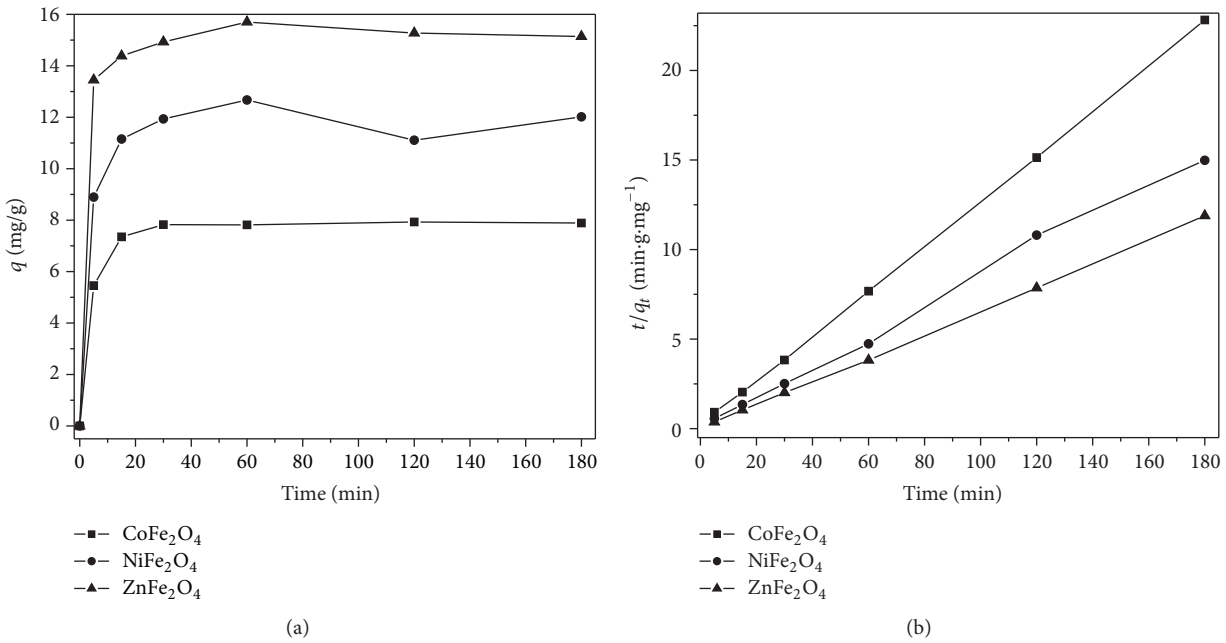

Figure 6: (a) Effect of contact time on the Pb(II) absorption by nanoferrites. (b) Pseudo-second-order sorption kinetics of Pb(II) sorption by MFe_2O_4 ferrite.

presence of a large number of vacant sites and, as a result, to an enhancement in the concentration gradient that is created between the adsorbate in the solution and the adsorbate in the adsorbent surface. After 60 min of contact time, this gradient is reduced due to the accumulation of Pb(II) on the vacant sites, causing a decrease in the adsorption gradient. The experimental data were fitted to the pseudo-first-order and pseudo-second-order models (Figure 6(b)). $q_{e,\mathrm{calc}}$ values of the calculated equilibrium sorption capacity in the case of the second-order model are very close to experimental $q_{e,\mathrm{exp}}$ values. In addition, based on the values of the correlation coefficient which is above 0.99, the second-order kinetic model was suitable to describe the adsorption process for Pb(II) adsorption (Table 1). It can be noted that the pseudo-second-order rate constant for $ZnFe_2O_4$ is higher than the other ferrites. This result can be attributed to the rapid redox reaction occurred between Pb species and the external adsorbent surface [45].

3.3. Isotherms. Figure 7 illustrates the plot of equilibrium concentrations of Pb(II) ions in the solid ($ZnFe_2O_4$, $NiFe_2O_4$, and $CoFe_2O_4$) and aqueous phases. The experimental data were fitted to the linear forms of the Langmuir and Freundlich isotherms. The values of the correlation coefficients (R^2) of the Langmuir isotherm model fit are above 0.99, indicating a good fit with the experimental data. The values of the isotherm constants are presented in Table 2. This confirms that the sorption occurred in the monolayer. This model assumes that a monolayer adsorption depends on the active sites of the adsorbent surface and there is no interaction between adsorbed species. Therefore, it can be concluded that the metal adsorption on the nanoparticles is possibly a physical adsorption process.

4. Conclusions

In summary, we investigated the effectiveness of $CoFe_2O_4$, $NiFe_2O_4$, and $ZnFe_2O_4$ ferrite nanoparticles for removing lead from aqueous solution. MFe_2O_4 (M = Co, Ni, and Zn) nanoparticles were successfully synthesized using a mechanochemical method. The formation of single-phase nanosized powders was confirmed by XRD analysis as well as IR and Raman spectroscopy. Magnetic measurements show that only $NiFe_2O_4$ and $ZnFe_2O_4$ samples exhibit superparamagnetic behavior at room temperature, whereas $CoFe_2O_4$ is ferromagnetic. The nanoparticles were effectively used to remove lead ions from aqueous solution, $ZnFe_2O_4$being the most efficient, followed by $NiFe_2O_4$ and $CoFe_2O_4$. Samples

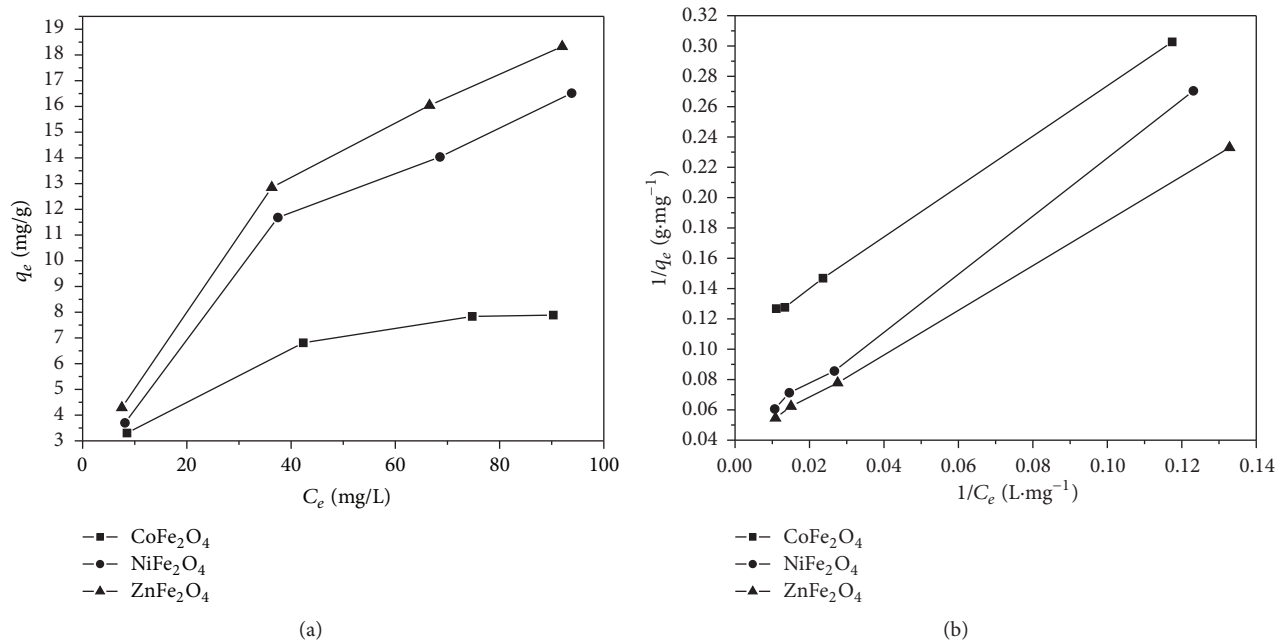

Figure 7: (a) Pb(II) adsorption isotherm on MFe_2O_4 ferrite. (b) Langmuir adsorption isotherm plot.

Table 2: Parameters obtained from the Langmuir model that describes the sorption of Pb^{2+} for $ZnFe_2O_4$, $NiFe_2O_4$, and $CoFe_2O_4$.

Adsorbent type	Langmuir Isotherm model		
	K_L (dm^3·mg^{-1})	q_m (mg·g^{-1})	R^2
$CoFe_2O_4$	0.064	9.34	0.99
$NiFe_2O_4$	0.061	17.76	0.99
$ZnFe_2O_4$	0.061	20.58	0.99

that present superparamagnetism at room temperature seem to have a better Pb(II) adsorption.

Competing Interests

The authors declare that they have no competing interests.

Acknowledgments

The authors acknowledge the financial support provided by CONACyT (Grants nos. CB-169133, 230530, and 128460), SEP, and VIEP-BUAP.

References

[1] R. Valenzuela, "Novel applications of ferrites," *Physics Research International*, vol. 2012, Article ID 591839, 9 pages, 2012.

[2] P. S. Antonel, C. L. P. Oliveira, G. A. Jorge, O. E. Perez, A. G. Leyva, and R. M. Negri, "Synthesis and characterization of $CoFe_2O_4$ magnetic nanotubes, nanorods and nanowires. Formation of magnetic structured elastomers by magnetic field-induced alignment of $CoFe_2O_4$ nanorods," *Journal of Nanoparticle Research*, vol. 17, article 294, 2015.

[3] A. Singh, A. Singh, S. Singh, P. Tandon, B. C. Yadav, and R. R. Yadav, "Synthesis, characterization and performance of zinc ferrite nanorods for room temperature sensing applications," *Journal of Alloys and Compounds*, vol. 618, pp. 475–483, 2015.

[4] S. Singh, P. Srivastava, and G. Singh, "Nanorods, nanospheres, nanocubes: synthesis, characterization and catalytic activity of nanoferrites of Mn, Co, Ni, Part-89," *Materials Research Bulletin*, vol. 48, no. 2, pp. 739–746, 2013.

[5] E. R. Kumar, P. S. P. Reddy, G. S. Devi, and S. Sathiyaraj, "Structural, dielectric and gas sensing behavior of Mn substituted spinel MFe_2O_4 (M= Zn, Cu, Ni, and Co) ferrite nanoparticles," *Journal of Magnetism and Magnetic Materials*, vol. 398, pp. 281–288, 2016.

[6] S. Joshi, V. B. Kamble, M. Kumar, A. M. Umarji, and G. Srivastava, "Nickel substitution induced effects on gas sensing properties of cobalt ferrite nanoparticles," *Journal of Alloys and Compounds*, vol. 654, pp. 460–466, 2016.

[7] A. A. Bagade and K. Y. Rajpure, "Development of $CoFe_2O_4$ thin films for nitrogen dioxide sensing at moderate operating temperature," *Journal of Alloys and Compounds*, vol. 657, pp. 414–421, 2016.

[8] A. Shan, X. Wu, J. Lu, C. Chen, and R. Wang, "Phase formations and magnetic properties of single crystal nickel ferrite ($NiFe_2O_4$) with different morphologies," *CrystEngComm*, vol. 17, no. 7, pp. 1603–1608, 2015.

[9] G. H. Jaffari, A. K. Rumaiz, J. C. Woicik, and S. I. Shah, "Influence of oxygen vacancies on the electronic structure and magnetic properties of $NiFe_2O_4$ thin films," *Journal of Applied Physics*, vol. 111, no. 9, Article ID 093906, 2012.

[10] W. S. Galvão, D. M. A. Neto, R. M. Freire, and P. B. A. Fechine, "Super-paramagnetic nanoparticles with spinel structure: a review of synthesis and biomedical applications," *Solid State Phenomena*, vol. 241, pp. 139–176, 2016.

[11] X. Piao, G. M. Zeng, D. L. Huang et al., "Use of iron oxide nanomaterials in wastewater treatment: a review," *Science of the Total Environment*, vol. 424, pp. 1–10, 2012.

[12] D. H. K. Reddy and Y. S. Yun, "Spinel ferrite magnetic adsorbents: alternative future materials for water purification?" *Coordination Chemistry Reviews*, vol. 315, pp. 90–111, 2016.

[13] A. K. Gupta and M. Gupta, "Synthesis and surface engineering of iron oxide nanoparticles for biomedical applications," *Biomaterials*, vol. 26, no. 18, pp. 3995–4021, 2005.

[14] Y. C. Sharma, V. Srivastava, V. K. Singh, S. N. Kaul, and C. H. Weng, "Nano-adsorbents for the removal of metallic pollutants from water and wastewater," *Environmental Technology*, vol. 30, no. 6, pp. 583–609, 2009.

[15] S. Chowdhury and R. Balasubramanian, "Recent advances in the use of graphene-family nanoadsorbents for removal of toxic pollutants from wastewater," *Advances in Colloid and Interface Science*, vol. 204, pp. 35–56, 2014.

[16] M. Hua, S. Zhang, B. Pan, W. Zhang, L. Lv, and Q. Zhang, "Heavy metal removal from water/wastewater by nanosized metal oxides: a review," *Journal of Hazardous Materials*, vol. 211-212, pp. 317–331, 2012.

[17] X. Hou, J. Feng, X. Liu et al., "Synthesis of 3D porous ferromagnetic $NiFe_2O_4$ and using as novel adsorbent to treat wastewater," *Journal of Colloid and Interface Science*, vol. 362, no. 2, pp. 477–485, 2011.

[18] N. Sezgin, M. Sahin, A. Yalcin, and Y. Koseoglu, "Synthesis, characterization and, the heavy metal removal efficiency of MFe_2O_4 (M=Ni, Cu) nanoparticles," *Ekoloji*, vol. 22, no. 89, pp. 89–96, 2013.

[19] F. Fu and Q. Wang, "Removal of heavy metal ions from wastewaters: a review," *Journal of Environmental Management*, vol. 92, no. 3, pp. 407–418, 2011.

[20] D. Mehtaa, S. Mazumdarb, and S. K. Singha, "Magnetic adsorbents for the treatment of water/wastewater—a review," *Journal of Water Process Engineering*, vol. 7, pp. 244–265, 2015.

[21] P. Sivakumar, R. Ramesh, A. Ramanand, S. Ponnusamy, and C. Muthamizhchelvan, "Synthesis and characterization of $NiFe_2O_4$ nanoparticles and nanorods," *Journal of Alloys and Compounds*, vol. 563, pp. 6–11, 2013.

[22] M. G. Naseri, E. B. Saion, and A. Kamali, "An overview on nanocrystalline$ZnFe_2O_4$, $MnFe_2O_4$ and $CoFe_2O_4$ synthesized by a thermal treatment method," *ISRN Nanotechnology*, vol. 2012, Article ID 604241, 11 pages, 2012.

[23] J. Fu, J. Zhang, Y. Peng et al., "Unique magnetic properties and magnetization reversal process of $CoFe_2O_4$ nanotubes fabricated by electrospinning," *Nanoscale*, vol. 4, no. 13, pp. 3932–3936, 2012.

[24] B. Aslibeiki, P. Kameli, M. H. Ehsani et al., "Synthesis of $MnFe_2O_4$ nanoparticles: The role of polymer coating on morphology and magnetic properties," *Journal of Magnetism and Magnetic Materials*, vol. 399, pp. 236–244, 2016.

[25] A. A. Bagade, V. V. Ganbavle, and K. Y. Rajpure, "Physicochemical properties of spray-deposited $CoFe_2O_4$ thin films," *Journal of Materials Engineering and Performance*, vol. 23, no. 8, pp. 2787–2794, 2014.

[26] A. Sutka, J. Zavickis, G. Mezinskis, D. Jakovlevs, and J. Barloti, "Ethanol monitoring by $ZnFe_2O_4$ thin film obtained by spray pyrolysis," *Sensors and Actuators B: Chemical*, vol. 176, pp. 330–334, 2013.

[27] M. M. Rahman, S. B. Khan, M. Faisal, A. M. Asiri, and K. A. Alamry, "Highly sensitive formaldehyde chemical sensor based on hydrothermally prepared spinel $ZnFe_2O_4$ nanorods," *Sensors and Actuators, B: Chemical*, vol. 171-172, pp. 932–937, 2012.

[28] J.-L. Li, Z. Yu, K. Sun, X.-N. Jiang, and Z.-W. Lan, "Structural and magnetic properties of $ZnFe_2O_4$ films deposited by low sputtering power," *International Journal of Minerals, Metallurgy, and Materials*, vol. 19, no. 10, pp. 964–968, 2012.

[29] E. Avvakumov, M. Senna, and N. Kosova, *Soft Mechanochemical Synthesis: A Basis for New Chemical Technologies*, Kluwer Academic Publishers, Boston, Mass, USA, 2001.

[30] Z. Ž. Lazarević, Č. Jovalekić, D. Sekulić et al., "Characterization of nanostructured spinel $NiFe_2O_4$ obtained by soft mechanochemical synthesis," *Science of Sintering*, vol. 44, no. 3, pp. 331–339, 2012.

[31] V. Šepelák, I. Bergmann, A. Feldhoff et al., "Nanocrystalline nickel ferrite, $NiFe_2O_4$: mechanosynthesis, nonequilibrium cation distribution, canted spin arrangement, and magnetic behavior," *The Journal of Physical Chemistry C*, vol. 111, no. 13, pp. 5026–5033, 2007.

[32] V. Šepelák, M. Menzel, K. D. Becker, and F. Krumeich, "Mechanochemical reduction of magnesium ferrite," *Journal of Physical Chemistry B*, vol. 106, no. 26, pp. 6672–6678, 2002.

[33] V. Šepelák, A. Feldhoff, P. Heitjans et al., "Nonequilibrium cation distribution, canted spin arrangement, and enhanced magnetization in nanosized $MgFe_2O_4$ prepared by a one-step mechanochemical route," *Chemistry of Materials*, vol. 18, no. 13, pp. 3057–3067, 2006.

[34] Z. Ž. Lazarević, C. Jovalekić, A. Milutinović et al., "Study of $NiFe_2O_4$ and $ZnFe_2O_4$ spinel ferrites prepared by soft mechanochemical synthesis," *Ferroelectrics*, vol. 448, no. 1, pp. 1–11, 2013.

[35] W. S. W. Ngah, S. Ab Ghani, and A. Kamari, "Adsorption behaviour of Fe(II) and Fe(III) ions in aqueous solution on chitosan and cross-linked chitosan beads," *Bioresource Technology*, vol. 96, no. 4, pp. 443–450, 2005.

[36] S. Rengaraj, K.-H. Yeon, and S.-H. Moon, "Removal of chromium from water and wastewater by ion exchange resins," *Journal of Hazardous Materials*, vol. 87, no. 1–3, pp. 273–287, 2001.

[37] http://www.crystalimpact.com/match.

[38] M. Günay, H. Erdemi, A. Baykal, H. Sözeri, and M. S. Toprak, "Triethylene glycol stabilized $MnFe_2O_4$ nanoparticle: Synthesis, magnetic and electrical characterization," *Materials Research Bulletin*, vol. 48, no. 3, pp. 1057–1064, 2013.

[39] Y. Koseoglu, F. Alan, M. Tan, R. Yilgin, and M. Öztürk, "Low temperature hydrothermal synthesis and characterization of Mn doped cobalt ferrite nanoparticles," *Ceramics International*, vol. 38, no. 5, pp. 3625–3634, 2012.

[40] V. A. M. Brabers, "Progress in spinel ferrite research," in *Handbook of Magnetic Materials*, K. H. J. Buschow, Ed., vol. 8, chapter 3, pp. 189–324, Elsevier, New York, NY, USA, 1995.

[41] A. Goldman, *Modern Ferrites Technology*, Springer, New York, NY, USA, 2nd edition, 2006.

[42] S. Sun, H. Zeng, D. B. Robinson et al., "Monodisperse MFe_2O_4 (M = Fe, Co, Mn) nanoparticles," *Journal of American Chemical Society*, vol. 126, no. 1, pp. 273–279, 2004.

[43] W. Wang, Z. Ding, X. Zhao et al., "Microstructure and magnetic properties of MFe_2O_4 (M = Co, Ni, and Mn) ferrite nanocrystals

prepared using colloid mill and hydrothermal method," *Journal of Applied Physics*, vol. 117, Article ID 17A328, 4 pages, 2015.

[44] D. Gherca, N. Cornei, O. Mentré, H. Kabbour, S. Daviero-Minaud, and A. Pui, "In situ surface treatment of nanocrystalline MFe_2O_4 (M = Co, Mg, Mn, Ni) spinel ferrites using linseed oil," *Applied Surface Science*, vol. 287, pp. 490–498, 2013.

[45] J. Hu, I. M. C. Lo, and G. Chen, "Comparative study of various magnetic nanoparticles for Cr(VI) removal," *Separation and Purification Technology*, vol. 56, no. 3, pp. 249–256, 2007.